Supplementary Materials: Understanding Factors that Control the Structural (Dis)Assembly of Sulphur-Bridged Bimetallic Sites

Riyadh Alrefai, Henri Eggenweiler, Hartmut Schubert and Andreas Berkefeld

1   General Information

Bis(trifluoromethanesulfonyl)amine (HNTf$_2$, 99%, Acros Organics) was sublimed once before use. 1,1'-Diacetylferrocene (Fc'', TCI) and (η^5-C$_5$H$_5$)$_2$Co (ampouled under Ar, ABCR) were used as received. Benzoquinone was recrystallized 3 times from ethanol, sublimed twice (r.t., 10^{-3} mbar, static vacuum), and stored under argon. AgClO$_4$ and high-purity ferrocene (Fc) were obtained from Alfa Aesar, and Fc was sublimed once prior to use. nBu$_4$NPF$_6$ electrolyte (Alfa Aesar) was recrystallized 3 times from acetone/water and employed as a 0.1 M solution in 1,2-C$_6$H$_4$F$_2$ and MeCN. Acetonitrile (MeCN) for electrochemical experiments was dried over and distilled from CaH$_2$, than P$_2$O$_5$, and finally percolated through activated neutral alumina. 1,2-C$_6$H$_4$F$_2$ (ABCR) was percolated through activated neutral alumina, distilled and stored over activated neutral alumina. Hexane was obtained from an MBraun solvent purification system (SPS). Benzene, diethyl ether, pentane, THF, and toluene were predried over activated 3 Å molecular sieves and distilled from sodium benzophenone ketyl or potassium metal under argon. Stabilizer free CH$_2$Cl$_2$ was first distilled from P$_2$O$_5$, then K$_2$CO$_3$, and finally stored over activated basic alumina. C$_6$D$_6$ and THF-d$_8$ were dried over and distilled from NaK alloy. CDCl$_3$ and CD$_2$Cl$_2$ were dried over and vacuum transferred from 3 Å molecular sieves. All solvents were stored over 3 Å molecular sieves or activated neutral alumina (MeCN, 1,2-C$_6$H$_4$F$_2$) under argon. Molecular sieves and neutral alumina were activated by heating under dynamic vacuum (10^{-3} mbar) at 250°C for 24–48 hours.
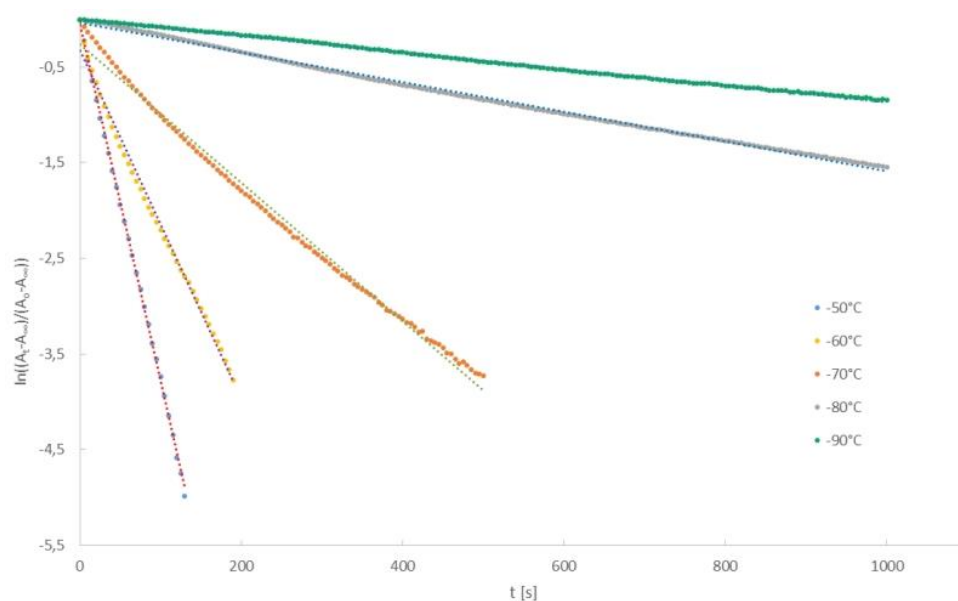
NMR data were recorded on Bruker Avance II 400, DRX 250, and Avance III HDX 600 instruments, and VT NMR spectra were recorded on a Bruker AVII+500 spectrometer. δ is given in ppm, *J* in Hz. ^{1}H

and $^{13}C\{^1H\}$ NMR chemical shifts are referenced to the residual ^1H and naturally abundance ^{13}C resonances of the solvents: δ =7.16/ 128.06 (C_6D_6), 1.72/ 67.21 (THF-d_8), 5.32/ 53.84 (CD_2Cl_2), and 7.26/ 77.16 ppm ($CDCl_3$). $^{31}P\{^1H\}$ NMR chemical shifts are referenced to an external standard sample of 85% H_3PO_4 set to δ = 0 ppm.
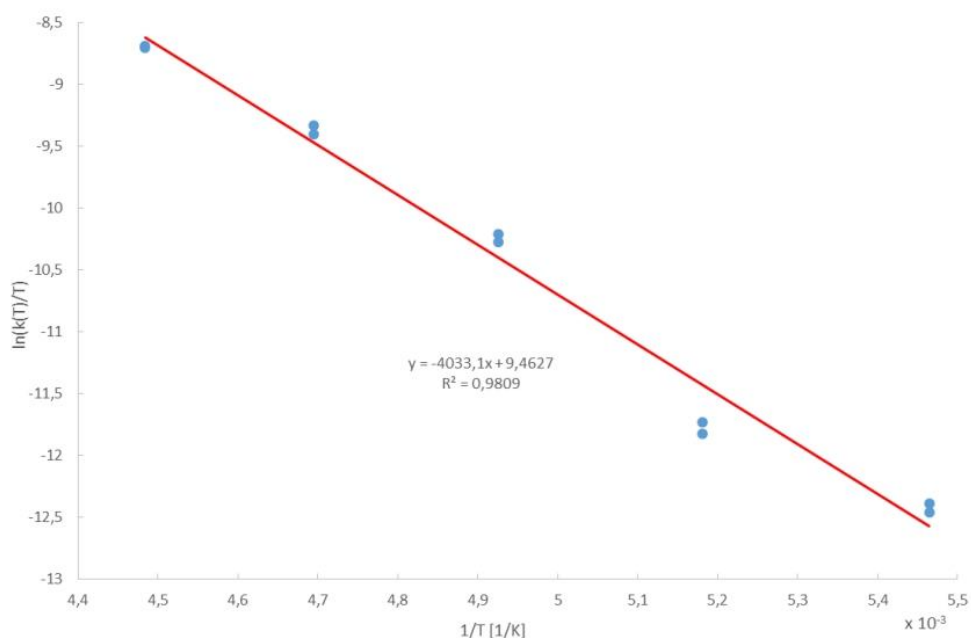
EPR spectra were collected using 4 mm O.D. Wilmad quartz (CFQ) EPR tubes on a continuous wave X-band Bruker ESP 300E spectrometer, and are referenced to the Bruker Strong Pitch standard g_{iso} = 2.0028. EPR simulations were done with EasySpin (version 5.0.21) and MATLAB and Statistic Toolbox Release R2015a (The MathWOrks, Inc., Natick, Massachusetts, United States). Fitting of EPR spectra was carried out with the easyfit tool included in EasySpin package [1], using either pepper for solid state or garlic for solution EPR data.

X-ray data were collected on a Bruker Smart APEXII diffractometer with graphite-monochromated MoKa radiation. The programs used were Bruker's APEX2 v2011.8-0, including SADABS for absorption correction and SAINT for structure solution, the WinGX suite of programs version 2013.3 [2], SHELXS and SHELXL for structure solution and refinement [3, 4], PLATON [5], and ORTEP [6]. Crystals were, unless otherwise noted, coated in a perfluorinated polyether oil and mounted on a 100 μm MiTeGen MicroMounts loop that was placed on the goniometer head under a stream of dry nitrogen at 100 K.
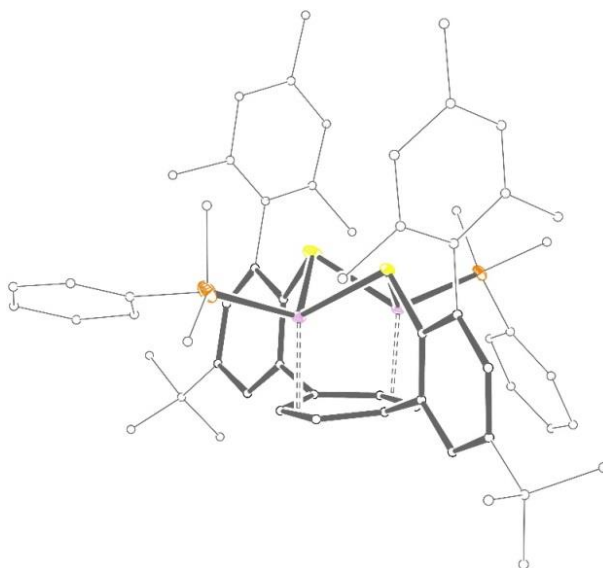
2   Supplementary Kinetic Data

Figure S1. Overview of temperature dependence of structural rearrangement of $[Ni_2(\mu\text{-S})_2]^{2+}$ into $[2\{\kappa\text{-S-Ni}\}_2]^{2+}$, represented by first order rate constant $k_d(T)$, in CH_2Cl_2 solution at $-90 \leq T \leq -50°C$; semilogarithmic plots of $\ln((A_t - A_\infty)/(A_{t=0} - A_\infty))$ vs time, A = absorbance at $\lambda = 715$ nm; Mean values from two independent runs: $k_d(-90°C) = (7.4 \pm 0.1)\times 10^{-4}$ s^{-1}, $k_d(-80°C) = (1.5 \pm 0.1)\times 10^{-3}$ s^{-1}, $k_d(-70°C) = (7.2 \pm 0.1)\times 10^{-3}$ s^{-1}, $k_d(-60°C) = (1.8 \pm 0.1)\times 10^{-2}$ s^{-1}, $k_d(-50°C) = (3.7 \pm 0.1)\times 10^{-2}$ s^{-1}.
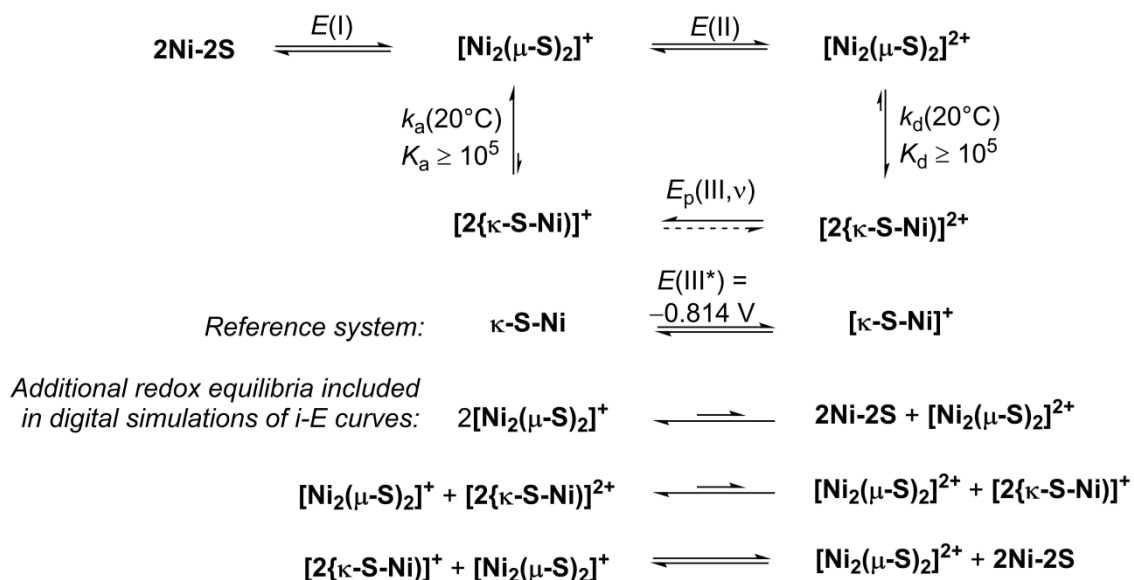

Figure S2. Determination of activation parameters $\Delta H^{\ddagger}_d$ and $\Delta S^{\ddagger}_d$ for structural rearrangement of $[Ni_2(\mu\text{-S})_2]^{2+}$ into $[2\{\kappa\text{-S-Ni}\}_2]^{2+}$ from linear regression of a semilogarithmic plot of $\ln(k_d(T))$, cf. Figure S1, vs $1/T$; rate constants $k_d(T)$ shown have been obtained from two independent runs, $\Delta H^{\ddagger}_d = (34 \pm 2)$ kJ mol^{-1}, $\Delta S^{\ddagger}_d = -(120 \pm 25)$ J mol^{-1} K^{-1}.

3   Supplementary Structural Data

Figure S3. Molecular connectivity plot as determined by X-ray diffraction of a single-crystalline sample of $[Ni_2(\mu\text{-}S)_2]N(SO_2CF_3)_2$; All atoms except for nickel, sulphur, and phosphorus refined isotropically; anisotropic displacement ellipsoids shown at 50 % probability level; H-atoms and counteranion omitted for clarity; color code: carbon = black, phosphorus = orange, nickel = plum, and sulphur = yellow.

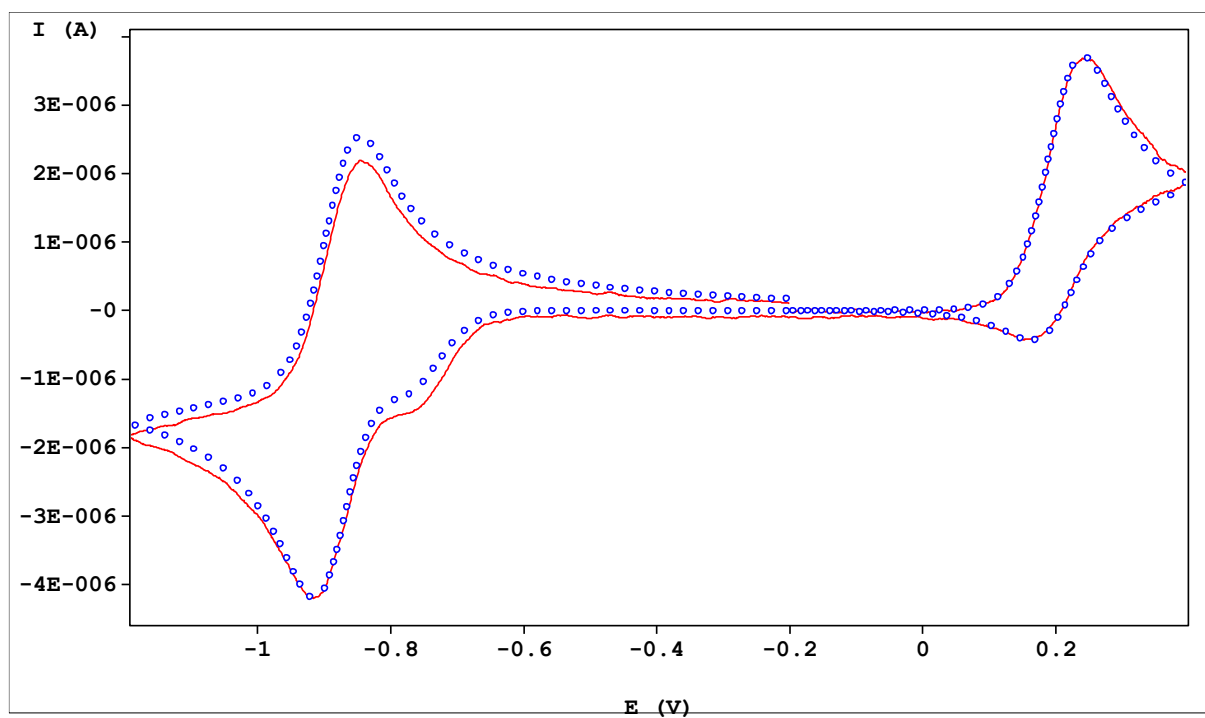## 4   Supplementary Electrochemical Data

Figure S4. Extended square scheme and additional redox equilibria included in digital simulation of cyclic current-potential curves.

Table S1. Parameters included in digital simulation of CV data; Fc = ferrocene.
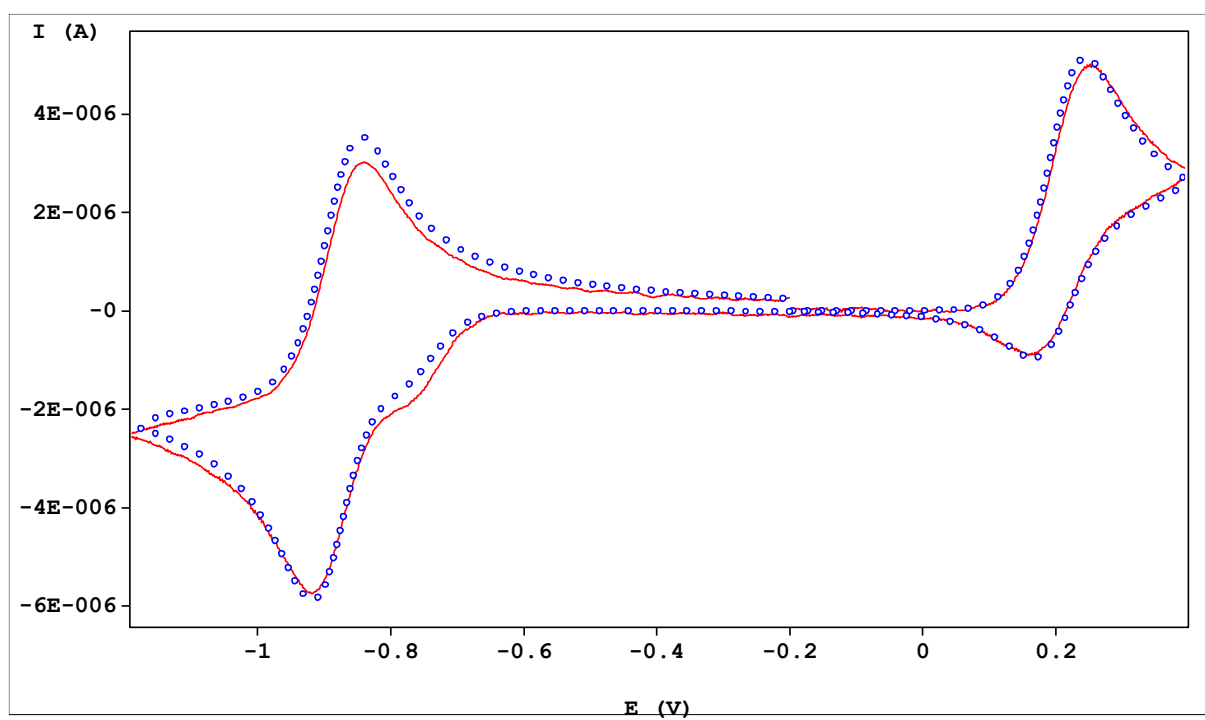
redox couple or reaction	E/V vs Fc/Fc$^+$	α	k_s/cm s^{-1}	D/10^{-6} cm^2 s^{-1}	K	k_{eq}/s^{-1}
[Ni$_2$(μ-S)$_2$]$^+$/ [Ni$_2$(μ-S)$_2$]$^{2+}$	0.207	0.55	0.012	3.8 3.9	-	-
[Ni$_2$(μ-S)$_2$]$^+$/ 2Ni-2S	−0.881	0.55	0.012	3.8 4.0	-	-
[2{κ-S-Ni}]$^{2+}$/ [2{κ-S-Ni}]$^+$	-	0.55	0.018	4.6 3.8	-	-
[Ni$_2$(μ-S)$_2$]$^{2+}$/ [2{κ-S-Ni}]$^{2+}$	-	-	-	-	≥ 10^8	10^4
[2{κ-S-Ni}]$^+$/ [Ni$_2$(μ-S)$_2$]$^+$	-	-	-	-	≥ 10^8	10^4
[κ-S-Ni]$^+$/ κ-S-Ni	−0.814	0.55	0.018	-	-	-

Table S2. Variation of k_a(20°C) estimated by digital simulation with potential sweep rate.

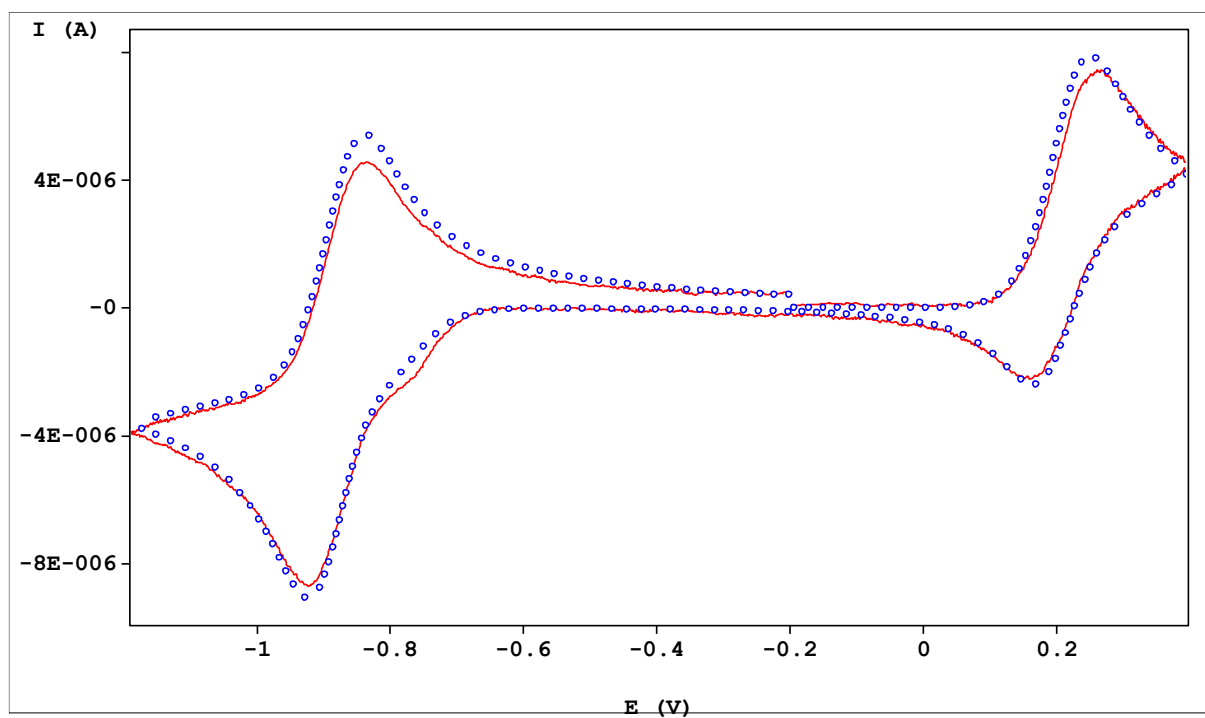| [Ni$_2$(μ-S)$_2$]$^{2+}$ → [2{κ-S-Ni}]$^{2+}$	k_a(20°C)/ s^{-1}	k_d(20°C)/ s^{-1}
50 mV s^{-1}	0.5	
100 mV s^{-1}	0.6	
200 mV s^{-1}	1.0	2800 ± 500
500 mV s^{-1}	1.5	
1000 mV s^{-1}	2.2	

Figure S5. Experimental (solid red) and digitally simulated (blue circles) cyclic current-potential curves at $\nu = 100$ mV s^{-1}, $c_0([\text{Ni}_2(\mu\text{-S})_2]\text{N}(\text{SO}_2\text{CF}_3)_2 = 261$ µM.
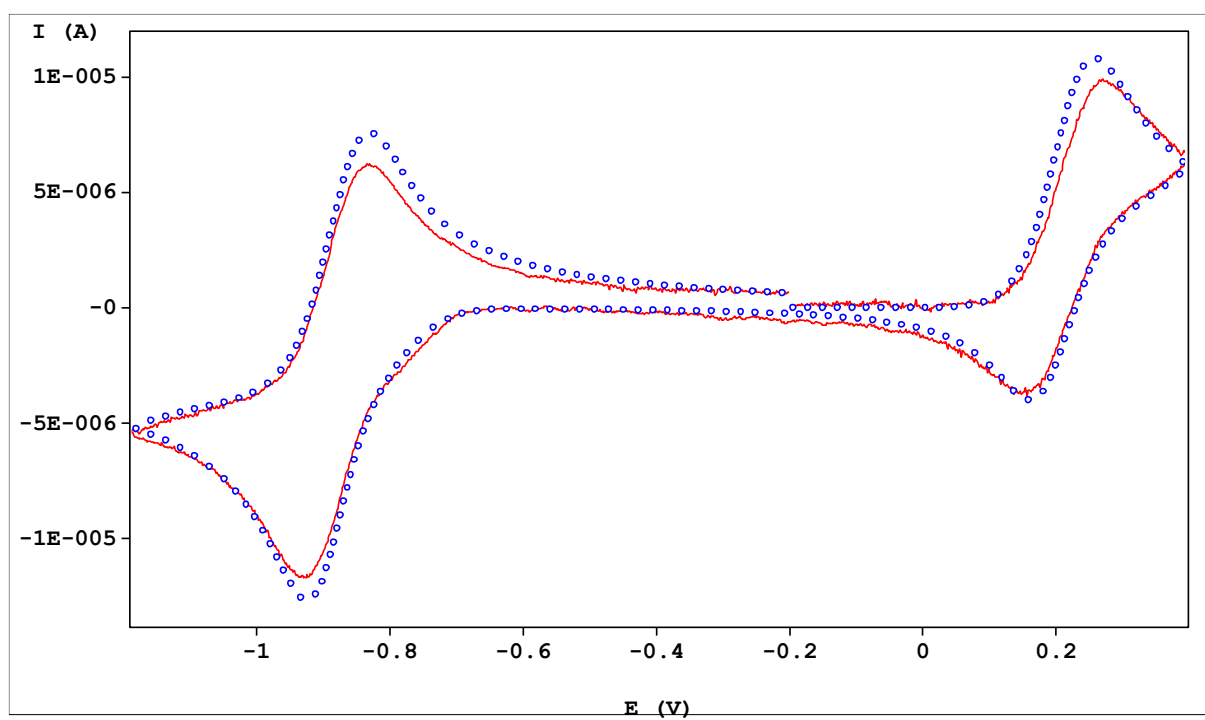

Figure S6. Experimental (solid red) and digitally simulated (blue circles) cyclic current-potential curves at $\nu = 200$ mV s^{-1}, $c_0([\text{Ni}_2(\mu\text{-S})_2]\text{N}(\text{SO}_2\text{CF}_3)_2 = 261$ µM.

Figure S7. Experimental (solid red) and digitally simulated (blue circles) cyclic current-potential curves at ν = 500 mV s^{-1}, c_0([Ni$_2$(μ-S)$_2$]N(SO$_2$CF$_3$)$_2$ = 261 μM.

Figure S8. Experimental (solid red) and digitally simulated (blue circles) cyclic current-potential curves at ν = 1000 mV s^{-1}, c_0([Ni$_2$(μ-S)$_2$]N(SO$_2$CF$_3$)$_2$ = 261 μM.

5   References

1.   Stoll, S.; Schweiger, A. EasySpin, a comprehensive software package for spectral simulation and analysis in EPR. *J. Magn. Res.* **2006**, 178, 42-55, https://doi.org/10.1016/j.jmr.2005.08.013.

2.   Farrugia, L. WinGX suite for small-molecule single-crystal crystallography. *J. Appl. Cryst.* **1999**, 32, 837-838, doi:10.1107/S0021889899006020.

3.   Hubschle, C. B.; Sheldrick, G. M.; Dittrich, B. ShelXle: a Qt graphical user interface for SHELXL. *J. Appl. Cryst.* **2011**, 44, 1281-1284, doi:10.1107/S0021889811043202.

4.   Sheldrick, G. A short history of SHELX. *Acta Cryst., A* **2008**, 64, 112-122, doi:10.1107/S0108767307043930.

5.   Spek, A. Structure validation in chemical crystallography. *Acta Cryst., D* **2009**, 65, 148-155, doi:10.1107/S090744490804362X.

6.   Farrugia, L. WinGX and ORTEP for Windows: an update. *J. Appl. Cryst.* **2012**, 45, 849-854, doi:10.1107/S0021889812029111.